Autocatalytic Mechanism of Pearlite Transformation in Steel

I. K. Razumov,[1,2,*] Yu. N. Gornostyrev,[1,2,4] and M. I. Katsnelson[3,4]

[1]*Institute of Metal Physics, UB of RAS, 18S. Kovalevskaya Street, Ekaterinburg 620990, Russia*
[2]*Institute of Quantum Materials Science, 5 Konstruktorov Street, Ekaterinburg 620072, Russia*
[3]*Radboud University, Institute for Molecules and Materials, Heyendaalseweg 135, Nijmegen 6525 AJ, Netherlands*
[4]*Ural Federal University, Department of Theoretical Physics and Applied Mathematics, 19 Mira Street, Ekaterinburg 620002, Russia*

(Received 25 May 2016; revised manuscript received 4 September 2016; published 3 January 2017)

A model of pearlite colony formation in carbon steels is developed, with a parametrization based on *ab initio* calculations. The model describes the processes of decomposition of austenite and formation of cementite through a metastable intermediate structure, with a crucial role of ferromagnetic order arising under the cooling. The autocatalytic mechanism of pearlite colony formation is analyzed and conditions for its implementation are established. We demonstrate that pearlite with lamellar structure is formed by the autocatalytic mechanism when thermodynamic equilibrium between the initial phase (austenite) and the products of its decomposition (cementite and ferrite) cannot be reached. The transformation diagram is suggested, and various scenarios of decomposition kinetics are investigated by phase-field simulations. By using a model expression for the free energy with first-principles parametrization, we find conditions of the formation of both lamellar and globular structures, in good agreement with experimental data.

DOI: 10.1103/PhysRevApplied.7.014002

I. INTRODUCTION

Pearlite is one of the main structural units of carbon steels which have a significant effect on their properties [1,2]. It is formed by the decomposition of austenite (γ phase, fcc Fe-C solid solution) into ferrite (α phase, bcc Fe) and cementite (orthorhombic θ phase, Fe_3C) during slow cooling or annealing at a temperature of 500–720 °C. The brightest feature of pearlite is a rather regular lamellar structure in which the α and θ phases are periodically alternated. Pearlite transformation (PT) is an example of eutectoid decomposition observed also in many nonferrous alloys [3–5] below some critical (eutectoid) temperature. Despite numerous studies of PT motivated by its great practical importance for metallurgy, the basic mechanisms of this transformation are still poorly understood.

The proposed theoretical models of PT are focused mostly on the stage of steady-state growth of the pearlite colony and on the problem of stability of the transformation front [6–13]. At the same time, the problems related to the early stages of the colony formation, such as nucleation of cementite, remain out of scope of the proposed models. In addition, the mechanism of lamellae multiplication by replication [1,14] or splitting [15], which plays an important role in PT, is still under discussion. The moving factors of the transition from lamellar to globular pearlite structure with increasing temperature are also not well understood [16–20].

There is a certain similarity between PT and other diffusion phase transformations resulting in the formation of the lamellar structure. The first example is eutectic colony growth which appears behind the front of solidification and is driven by the temperature gradient [21,22]. This transformation is controlled by fast diffusion at the solidification front and/or the decomposition of some intermediate states [23,24]. Another example is a spinodal decomposition driven by the moving grain boundary (GB) in systems with negative mixing energy, $v < 0$ [25]. The stability of the transformation front is naturally protected in this case, and lamellar structure formation is controlled by the redistribution of alloying elements along the GB. These observations point out the importance of the acceleration of diffusion at the transformation front, as was discussed in relation to the PT problem (see Refs. [6,8,11]). It is worthwhile to note that despite the decisive role of redistribution of carbon in PT, the austenite remains stable with respect to the carbon decomposition, $v_\gamma > 0$ [26].

In this work, we demonstrate that the formation of the lamellar structure is a natural part of the scenario of PT when the free energy of the system has a special form, namely, when the thermodynamic equilibrium between the parent γ phase and both transformation products (α and θ) is impossible. In this case, the pearlite colony can emerge by some kind of autocatalytic mechanism when the appearance of one of the phases (α or θ) stimulates the nucleation of the other.

We employ the previously proposed model of phase transformation in iron and steel [27,28] and generalize it by

*rik@imp.uran.ru

taking into account the cementite formation. Following Ref. [29], we also assume that the metastable intermediate structure (MIS) arises at the $f_{\alpha Fe}(T) = f_\alpha(0,T)$ interface due to the magnetization growth induced by an adjacent ferrite plate; the nucleation of cementite occurs as the result of the MIS $\rightarrow \theta$ lattice reconstruction when the MIS is saturated by carbon. Thus, according to the scenario developed, PT at undercooling results initially from the arising magnetic order in the α phase. It is worthwhile to note that the formation of the MIS is closely connected to the computational result (see Refs. [30,31]) that the ground state of ferromagnetically ordered γ-Fe has a strong tetragonal distortion.

II. METHODS

A. Effective free-energy functional

Here we generalize the previously proposed model [27,28] of the γ-α transformation by taking into account the cementite formation. In this approach, all relevant degrees of freedom (lattice and magnetic) as well as carbon diffusion and its redistribution during the γ-α and γ-θ phase transformations should be included. We assume that the nucleation of cementite occurs at the γ/α interface, and γ-θ lattice reconstruction follows the transformation path, which includes the formation of the MIS [29].

The pearlite formation is controlled by the carbon diffusion [1,2], which is a slow process, in contrast to γ-α and γ-MIS lattice reconstruction carried out by the fast cooperative displacements of Fe atoms. Therefore, we assume that variables describing the lattice reconstruction reach their equilibrium values quickly and that the local carbon concentration $c(\mathbf{r})$ remains a single variable determining the slow evolution.

Since the α and θ phases in pearlite colonies are usually conjugated with a small mismatch, whereas the lattice coherency is lost on the transformation front [32], we neglect the elastic energy contribution within the simple model under consideration. Thus, after excluding the fast variables, the effective free-energy functional takes the form [33]

$$F = \int \left(f_{\text{eff}}(c,T) + \frac{k_c}{2}(\nabla c)^2 \right) d\mathbf{r}, \qquad (1)$$

where $f_{\text{eff}}(c,T)$ is the effective free-energy density for a homogeneous state

$$f_{\text{eff}}(c,T) = \min\{f_\alpha(c,T), f_\gamma(c,T), f_\theta(c,T)\}, \qquad (2)$$

and $f_{\gamma(\alpha,\theta)}(c,T)$ is the local density of free energy of austenite (ferrite, cementite) at carbon concentration c and temperature T. This prescription means that the phase with the lowest energy at a fixed value of local carbon concentration is realized at a given space point. A similar approach to pearlite free energy was previously used in Ref. [11].

To determine the energies $f_{\gamma(\alpha)}(c,T)$, we use the earlier proposed model [28] taking into account both lattice and magnetic degrees of freedom. According to this model,

$$f_\gamma(c,T) = g_\gamma^{\text{PM}} - \int_0^{\tilde{J}_\gamma} Q(\tilde{J}'_\gamma, T) d\tilde{J}'_\gamma - T(s_0 + S_\gamma), \qquad (3)$$

$$f_\alpha(c,T) = g_\alpha^{\text{PM}} - \int_0^{\tilde{J}_\alpha} Q(\tilde{J}'_\alpha, T) d\tilde{J}'_\alpha - TS_\alpha, \qquad (4)$$

where s_0 is the high-temperature limit of the entropy difference (including phonon contribution) between the γ and α phases of elemental iron, and $S_{\alpha(\gamma)}$ is configurational entropy of carbon in the $\alpha(\gamma)$ phase. $Q(T) \equiv \langle \mathbf{m}_0 \cdot \mathbf{m}_1 \rangle / m^2$ is the spin-correlation function dependent on the temperature [we adopt the Q (T) dependence from the Oguchi model [34]], $\tilde{J}_{\gamma(\alpha)}(c) = g^{\text{PM}}_{\gamma(\alpha)}(c) - g^{FM}_{\gamma(\alpha)}(c)$ is the exchange energy,

$$\begin{aligned} g_\gamma^{\text{PM(FM)}}(c) &= \tilde{g}_\gamma^{\text{PM(FM)}} + \varepsilon_\gamma^{\text{PM(FM)}} c + v_\gamma c^2/2, \\ g_\alpha^{\text{PM(FM)}}(c) &= \tilde{g}_\alpha^{\text{PM(FM)}} + \varepsilon_\alpha^{\text{PM(FM)}} c + v_\alpha c^2/2. \end{aligned} \qquad (5)$$

$\tilde{g}^{\text{PM(FM)}}_{\gamma(\alpha)}$ are the energies of para- (ferro)magnetic elemental Fe found from the fitting to *ab initio* computational results [31,35], and $\varepsilon^{\text{PM(FM)}}_{\gamma(\alpha)}$ and $v_{\gamma(\alpha)}$ are the solution and mixing energies of carbon in the fcc (bcc) lattice, respectively. Because PT results in the cementite formation, the carbon concentration grows essentially and reaches the value $c = 0.25$. Therefore, the contribution proportional to c^2 characterizing carbon-carbon interactions is taken into account in Eq. (5). Note that within this model, a strong temperature dependence of the free energy of α-Fe originates from the increase of the degree of ferromagnetic order during the cooling rather than from the phonon entropy.

We use the traditional lattice-gas model to describe the statistical entropy of carbon randomly distributed over interstitials of α-Fe. It is a rather good approximation due to the very low solubility limit of carbon in the α phase, so the correlation effects are supposed to be negligible. Therefore, we assume that carbon atoms are rapidly redistributed over all three octahedral interstitial sublattices after the γ-α phase transition [33]. On the other hand, the solubility of carbon in the γ phase is much higher, and the correlation effects should be taken into account. Following Refs. [28,36,37], we take into account the repulsive interactions between the nearest-neighbor carbon atoms by assuming that only a quarter of the positions are available in fcc Fe.

Thus, the configurational entropy of carbon in the α and γ phase reads

$$S_\alpha \approx -kc\ln(c/3),$$
$$S_\gamma = -k[4c\ln(4c) + (1-4c)\ln(1-4c)]/4. \quad (6)$$

Following Ref. [38], the concentration dependence of the free-energy density of cementite has the form

$$f_\theta(c,T) = f_{\alpha\mathrm{Fe}}(T) + \Delta f_{\alpha\theta}(T) + \Delta f_\theta^{(1)}(c,T), \quad (7)$$

where $f_{\alpha\mathrm{Fe}}(T) = f_\alpha(0,T)$ is the free-energy density of pure α iron, $\Delta f_{\alpha\theta}(T)$ is the free-energy density of the formation of stoichiometric cementite from pure components (bcc Fe and graphite), which is known from CALPHAD [39] or *ab initio* calculations [40,41], $c_{\mathrm{cem}} = 0.25$ is the stoichiometric composition of cementite, and $\Delta f_\theta^{(1)}(c,T)$ is the variation of the free-energy density of cementite due to deviation from stoichiometry calculated in Ref. [38] within the model of the regular carbon-vacancy solution. The details of the parametrization of formulas (3)–(7) are presented in the Appendix.

Following the results of Ref. [29], we assume that the cementite nucleation occurs by a displacive mechanism in the ferromagnetic region which arises near the ferrite plate and propagates further into the bulk. Herewith, the MIS formed at the α/γ interface provides the easier and faster realization of the γ-θ phase transformation and maintains the lattice coherence. To take into account the MIS effect near the ferrite boundary, we replace the concentration dependence $f_\theta^{(1)}(c)$ [38] by an effective one, so that an intersection point of free energies $f_\gamma(c)$ and $f_\theta(c)$ shifts to the left by the value $\Delta c_{\mathrm{bound}} \sim 0.05$ (see explanations to Fig. 2 in Sec. III A). We also assume that the carbon concentration $c = 0.25$ is reached primarily in the bulk phase with higher carbon solubility, so the free-energy density $f_\theta(c_{\mathrm{cem}})$ remains unchanged.

B. Simulation of transformation kinetics

To study the evolution of the microstructure during PT, we numerically solve the nonlinear diffusion-type equation describing the distribution of carbon $c(\mathbf{r},t)$,

$$\frac{\partial c}{\partial t} = -\nabla\mathbf{I}, \qquad \mathbf{I} = -\frac{D(c)}{kT}c(1-c)\nabla\left(\frac{\delta F}{\delta c}\right), \quad (8)$$

where $F(c)$ is determined by Eq. (1). The carbon diffusion coefficient is defined as

$$D(c) = [D_\gamma + (D_\alpha - D_\gamma)h(C_{T0} - c)]h(C_{T1} - c) + D_\theta h(c - C_{T1}), \quad (9)$$

where $h(x)$ is a smoothed Heaviside step function, C_{T0}, C_{T1} are carbon concentrations corresponding to the conditions of paraequilibrium, that is, $f_\gamma(c,T) = f_\alpha(c,T)$ and $f_\gamma(c,T) = f_\theta(c,T)$, respectively. Thus, $D(c)$ equals D_α, D_γ, D_θ in the bulk of the corresponding phases and takes the intermediate values at the interfaces. The simulation is performed at the square grid 800×800 with mirror-symmetric boundary conditions [42] by using the Runge-Kutta procedure. Such choice of the boundary conditions allows us to model the formation of a single isolated pearlite colony in the considered area. To simulate the nucleation of the colony, we choose the initial state as the γ phase with a homogeneous carbon concentration and introduce there a small embryo of ferrite or cementite phase.

III. RESULTS

A. Transformation diagram

The local density of free energy of each phase $f_{\alpha(\gamma,\theta)}(c)$ calculated for different temperatures by using the model described above [Eqs. (3)–(7)] are shown in Figs. 1(a) and 1(b) together with the effective local density of free energy $f_{\mathrm{eff}}(c) = \min\{f_\alpha(c), f_\gamma(c), f_\theta(c)\}$ [Fig. 1(c)].

After the exclusion of the fast variables, the carbon concentration is the only quantity that determines the phase state of Fe-C, and it plays the role of an order parameter. As one can see from Fig. 1(a), at $T = 750$ K, ferrite and cementite are preferred for $c < 0.027$ and $c > 0.20$, respectively; within the interval $0.027 < c < 0.20$, austenite is energetically preferable.

The realization of the MIS on the $\gamma \to \theta$ transformation pathway [29] facilitates the nucleation of cementite near the α/γ interface due to the magnetization induced by an adjacent ferrite plate. As a result, the $\gamma \to \theta$ transformation starts near the ferrite plate when reaching smaller carbon concentrations [about 15 at. %; see Fig. 1(b)] in comparison with the bulk. We assume that stoichiometric cementite ($c = 0.25$) exists in a paramagnetic state, and it has the same energy in the bulk and near the ferrite plate as well, since the tendency to magnetic order decreases with the carbon concentration increase. Thus, we consider an effective $\gamma \to \theta$ transformation pathway, taking into account the nucleation of cementite on the ferrite plate [curve 3 in Fig. 1(b)].

Above the eutectoid temperature $T_{\mathrm{eutec}} = 1000$ K, two-phase equilibria $\gamma + \theta$ and $\gamma + \alpha$ take place [curve 1 in Fig. 1(c)]. When the temperature decreases, the γ phase becomes metastable with respect to the decomposition to the θ and α phases, wherein a stable equilibrium α/θ arises [curve 2 in Fig. 1(c)]. With the further decrease of the temperature, below some critical value, all metastable equilibria disappear [curve 3, Fig. 1(c)], and the only stable two-phase $\alpha + \theta$ state survives.

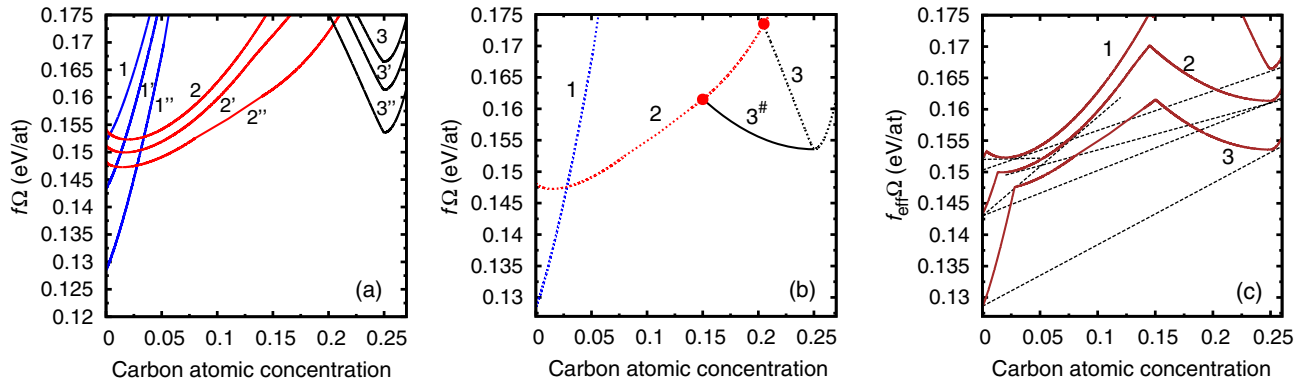

FIG. 1. Variants of the phase equilibrium in the Fe-C system with triple-well thermodynamic potential $f(c)$. (a) Calculated density of the free energy of the α (blue), γ (red), θ (black) phases in the model with *ab initio* parametrization at $T = 1050$ K (1–3), 900 K (1'–3'), 750 K (1"–3"); Ω is the volume per atom of iron. (b) Change in the conditions of cementite formation near the ferrite boundary at 750 K, free-energy density of the α, γ, θ phases (1–3), and the effective free-energy density of cementite ($3^{\#}$). (c) Resulting effective density of free energy as a function of carbon concentration at $T = 1050$ K (1), 900 K (2), 750 K (3); dotted lines are tangents to the free energies of the phases.

These changes in equilibrium conditions result in different scenarios of austenite decomposition. It is convenient to present them using the transformation diagram (Fig. 2) proposed earlier in Ref. [28], with also adding the PT. In this diagram, the lines A_3 and A_{CM} are boundaries of two phase regions $\gamma + \alpha$ and $\gamma + \theta$, respectively, and are constructed from the condition of equality of the chemical potentials of carbon in the corresponding phases. The lines T_0 and T_1^{bulk} correspond to the γ/α and γ/θ paraequilibrium condition when the free energies of the γ, α or γ, θ phases with the same carbon concentration become equal; these lines coincide with the temperature dependence of the intersection points of free-energy densities of the considered phases [see Fig. 1(a)]. The intersection point of the austenite and PM cementite energies T_1^{bulk} shifts to the right up to the value $c \sim 0.24$ achieved at low temperature. The intersection point of the MIS and FM cementite energies T_1^{bound} is approximately $c \sim 0.18$ at $T = 0$ K according to Ref. [29]. We suppose that the dependences $T_1^{\mathrm{bulk}}(T)$ and $T_1^{\mathrm{bound}}(T)$ are similar so that the line $T_1^{\mathrm{bound}}(T)$ can be constructed by shifting the line $T_1^{\mathrm{bulk}}(T)$ to the left by $\Delta c_{\mathrm{bound}} \sim 0.05$. This line describes the nucleation of cementite near the α/γ interface provided by the MIS.

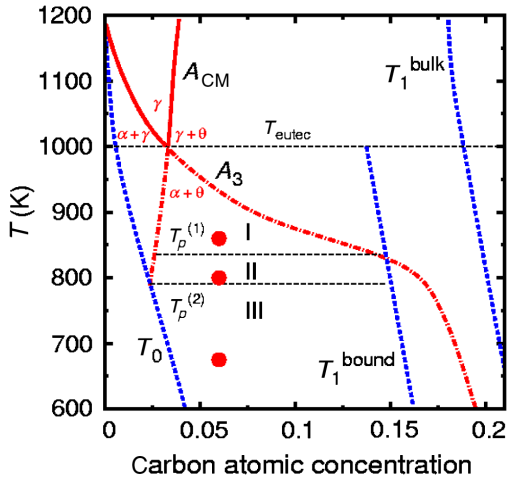

FIG. 2. The calculated transformation diagram. The lines A_3 and A_{CM} are the boundaries of two-phase regions $\alpha + \gamma$ and $\gamma + \theta$ as well as their metastable extensions below the eutectoid temperature T_{eutec}; the lines T_0 and T_1 are lines of instability with respect to the $\gamma \to \alpha$ and $\gamma \to \theta$ transformations, respectively. The temperature regions I–III are determined by the intersection points of these lines. The circles indicate the conditions under which the simulations are carried out.

Below the eutectoid temperature T_{eutec}, the decomposition $\gamma \to \alpha + \theta$ is possible. As suggested in Refs. [43,44], the development of PT is expected below T_{eutec} within a window between the metastable extensions of the lines A_3 and A_{CM} (corresponding to metastable equilibria γ/α and γ/θ, respectively), where austenite is supersaturated with respect to both the α and θ phases. In this region, the formation of one of the phases (α or θ) will stimulate the appearance of another one and, therefore, results in pearlite formation. Here we develop this view and show that this region can be divided into three subdomains I–III where the kinetics of PT is rather different. In region I, both metastable equilibria γ/α and γ/θ can be reached [see Fig. 1(c), curve 2]. In region II, only the metastable equilibrium γ/θ survives. Finally, in region III, the metastable equilibria between austenite (γ) and both transformation products (α and θ) are impossible [Fig. 1(c), curve 3]. In the latter case, we expect that the appearance one phase (α or θ) will stimulate the fast formation of the other one. However, the simulation of the decomposition kinetics is required to study the microstructure morphology.

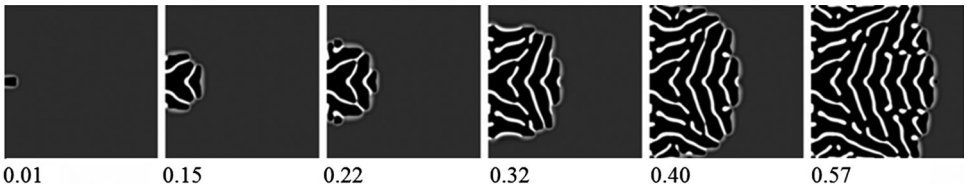

FIG. 3. Kinetics of lamellar structure growth from a single ferrite nucleus placed on the grain boundary; $T = 675$ K, $c_0 = 0.06$. The numbers under each fragment correspond to the dimensionless simulation time. The different levels of carbon concentrations are shown by gray scale, wherein cementite is white and ferrite is black.

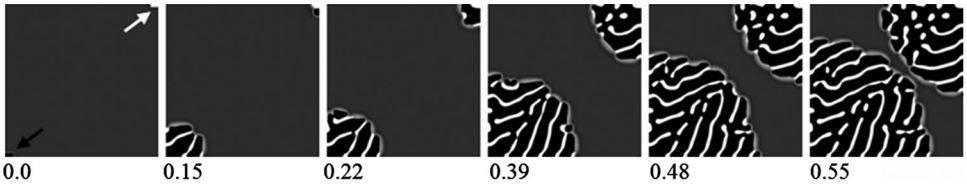

FIG. 4. Kinetics of lamellar structure growth from a nucleus placed on the grain boundaries' junctions (ferrite nucleus in the bottom left and cementite nucleus in the upper right corner are indicated by arrows); $T = 675$ K, $c_0 = 0.06$.

B. Simulation of PT. Lamellar and globular pearlite

To specify the morphology of the transformation product, we carry out phase-field simulations of PT starting from the homogeneous initial state with a single small ferrite nucleus. We find that below a temperature $T_p^{(1)}$ two scenarios of PT are possible, leading to the formation of either globular (region II) or lamellar structure (region III). The corresponding results are presented in Figs. 3–6. The different levels of carbon concentrations are shown by gray scale, wherein cementite is white and ferrite is black. The time is given in dimensionless units L^2/D_α, where the square side is $L = 1$ mkm (see the Appendix).

In region III, a fine and rather regular lamellar structure is formed regardless of the location of initial embryo (Figs. 3 and 4). In this case, as the first step, carbon is pushed out from the embryo of ferrite, and its concentration near the ferrite interface reaches the threshold value $c(T_1^{\text{bound}})$. After this, the MIS $\rightarrow \theta$ transformation occurs at the interface, and the carbon flow from the γ matrix provides saturation of the θ phase and depletion of carbon in the surrounding austenite. Since cementite cannot be in equilibrium with the γ matrix in this region of the diagram, the process continues until the critical concentration $c(T_0)$ is reached. After that, a new ferrite layer is formed near the θ phase, and the process described above repeats so that the corresponding mechanism can be called autocatalytic. Phase-field simulations show that the front movement of the pearlite colony is accompanied by an increase of its transverse size. As a result, the pearlite colony gets a fan-type shape, in agreement with the experimental data [1,19]. Herewith, the lamellae do not have a well-marked tendency of normal orientation to the transformation front. At the late stages, the space is filled by the ferrite domains, and the allocation of lamellae is well correlated within each domain. One can assume that the elastic stresses, which are not taken into account here, provide even more regular structures.

Note that a similar pearlite structure can also arise in region III if we start from one cementite embryo instead of ferrite (see Fig. 4, upper right corner).

The position of the start line T_1^{bound} of the $\gamma \rightarrow \theta$ transformation (see Fig. 2) is partly controversial since the results [29] are obtained at $T = 0$ K. Therefore, we perform the calculation at various positions of T_1^{bound}. Figure 5 represents the simulation results when choosing the parameters analogous to Fig. 4, but the line T_1^{bound} is additionally shifted to the left. It results in the formation of a more regular lamellar structure with a smaller interlamellar spacing because carbon extraction from a smaller volume is required to reach the smaller critical concentration C_{T1} near the ferrite plate, at which the realization of cementite nucleation takes place. Otherwise, the shift of the line T_1^{bound} to the right leads to decreasing the critical temperature of autocatalysis $T_p = \min\{T_p^{(1)}, T_p^{(2)}\}$ and to a coarsening of the microstructure; the corresponding kinetics pictures are not presented here.

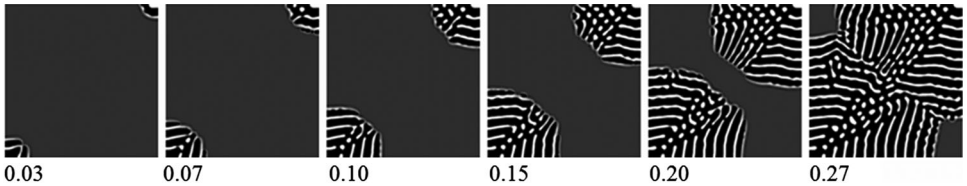

FIG. 5. Kinetics of lamellar structure growth at shifting the line T_1 to the left by $\delta c = 0.03$. The other parameters are the same as in Fig. 4.

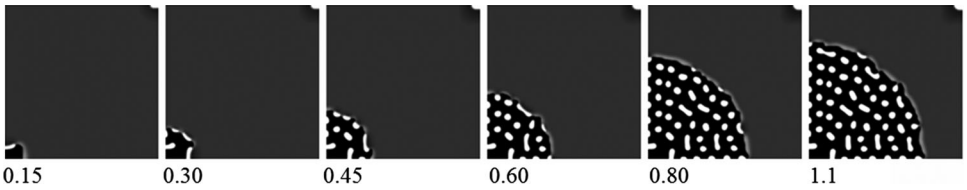

FIG. 6. Kinetics of globular structure growth; $T = 800$ K, and the other parameters are the same as in Fig. 4.

In region II, PT starts only with ferrite embryos, since they alone cannot be in equilibrium with austenite. In this case, the condition of the autocatalytic multiplication of lamellae is violated, and the phase-field simulation demonstrates a coarse globular structure (Fig. 6). As in the previous case, carbon is pushed out from the embryo of ferrite, and the chain of transformations $\gamma \rightarrow \mathrm{MIS} \rightarrow \theta$ is realized. However, in this case, the line A_{CM} is achieved before the critical concentration $c(T_0)$ so that the metastable-phase equilibrium γ/θ is realized, and the new ferritic layer does not appear. As a result, the other scenario of transformation takes place which results in numerous small cementite precipitates in the single ferritic matrix.

In region I in Fig. 2, austenite is decomposed by the conventional nucleation-and-growth mechanism as discussed in Ref. [28] (the corresponding pictures are not shown here). Carbon is pushed out from the ferrite embryo, and its concentration near the ferrite interface reaches the value determined by the A_3 curve. Since $c(A_3) < c(T_1^{\mathrm{bound}})$, the local metastable-phase equilibrium α/γ is reached, and the formation of cementite does not occur in this case. And vice versa, if we start from one cementite embryo, the local metastable-phase equilibrium γ/θ is realized, and ferrite does not occur because $c(A_{\mathrm{CM}}) > c(T_0)$.

We also consider the effect of variation of the diffusion coefficients, and we find that the interlamellar spacing increases with increasing the parameter D_α/D_γ. However, this effect is negligible due to the small carbon solubility in ferrite so that the variation of carbon diffusion in ferrite does not change the microstructure up to very high values of D_α/D_γ.

IV. DISCUSSION

The proposed model based on *ab initio* parametrization describes all the most essential features of PT. In particular, the model predicts the autocatalytic scenario of quite regular pearlite colony formation and the change in pearlite morphology from lamellar to globular when the temperature increases above some critical value $T_p^{(2)}$. It is in agreement with the experimental observations of globular and lamellar pearlite transformations [16–19], and the former takes place at smaller undercooling temperatures. Note that the free energies of each phase depend on steel composition, and the alloying affects the position of regions I and II.

The suggested mechanism of the autocatalytic PT has some similarity to the spinodal decomposition of alloys but has also essentially new features. Namely, the austenite remains stable with respect to small fluctuations of carbon concentration, and only the formation of ferrite plates stimulates the local saturation of carbon and cementite nucleation. Note that the autocatalytic decomposition of some metastable phases was considered earlier in Refs. [11,45].

Within the approach under consideration, the instability of austenite with respect to $\gamma \rightarrow \alpha + \theta$ decomposition develops stepwise with the temperature decrease. The existence of the threshold temperature of autocatalysis is consistent with the available experimental data [46,47]. For example, according to Ref. [47], the pearlite nucleation rate (in contrast to the growth rate) is close to zero at $T_p^{\mathrm{exp}} < T < T_{\mathrm{evtec}}$ and increases abruptly at T_p^{exp} ($T_p^{\mathrm{exp}} = 820$ K is start temperature of the fast pearlite transformation). Similar behavior is discussed in Ref. [46] where a narrower temperature interval with the close-to-zero nucleation rate is observed.

An important element of the proposed model is the assumption that the nucleation of cementite is facilitated near the α/γ interface due to magnetization induced by an adjacent ferrite plate. We assume that the MIS emerging at the α/γ interface due to an increase of magnetic order in the α phase plays a decisive role in the formation of cementite and provides fast lattice reconstruction during the autocatalytic PT.

The model is rather simple and does not take into account a real geometry of conjugation of the α and θ phases, as well as an elastic strain due to lattice mismatch. Nevertheless, this approach allows us to construct a realistic transformation diagram and investigate the kinetics of pearlite colony formation. The results may also be important to eutectic or eutectoid growth of colonies in other systems.

ACKNOWLEDGMENTS

The research is carried out within the state assignment of The Federal Agency for Scientific Organizations of Russia (theme "Magnet" N01201463328) and partially supported by Act 211 of the government of the Russian Federation, Contract No. 02.A03.21.0006. M. I. K. acknowledges support from Nederlandse Organisatie voor Wetenschappelijk Onderzoek via the Spinoza grant.

APPENDIX: DETAILS OF PARAMETRIZATION

We use the dissolution and mixing energies of carbon close to those known from experimental data and *ab initio* calculations: $\varepsilon_\alpha^{\mathrm{FM}} = 0.9$ [37,47,48], $\varepsilon_\alpha^{\mathrm{PM}} = 0.9$

[48], $\varepsilon_\gamma^{\mathrm{PM}} = 0.3$ [49,50], $\varepsilon_\gamma^{\mathrm{FM}} = -0.4$ [28,48], $v_\alpha = 6$ [26], and $v_\gamma = 1.5$ [26,50]] (in eV/at.). The estimations of v_γ vary greatly from 1 to 3 eV/at; the values $\varepsilon_\alpha^{\mathrm{PM}}$, $\varepsilon_\gamma^{\mathrm{FM}}$ are known only from *ab initio* calculations, and the difference between the *ab initio* and experimental estimations of $\varepsilon_\alpha^{\mathrm{FM}}$, $\varepsilon_\gamma^{\mathrm{PM}}$ is about 0.2 eV/at. Note that the γ phase is stable with respect to small concentration fluctuations since $v_\gamma > 0$, and the value of v_α is not essential since the carbon solubility in the phase is very small. We neglect the dependence of energies $\varepsilon_{\gamma(\alpha)}^{\mathrm{FM(PM)}}$ on the temperature, which is partly compensated by the choice of its changed values (within a pointed-out error, 0.2 eV/at).

The temperature dependence of the difference between the cementite and ferrite free energies $\Delta f_{\alpha\theta}(T)$ is chosen close to the CALPHAD and *ab initio* calculations [39–41], with the additional condition that the curve A_{CM} passes through the eutectoid point ($c = 0.034$, $T = 1000$ K), $\Delta f_{\alpha\theta}(T) = 0.109\text{–}0.173\tau_c + 0.078\tau_c^2$ (in eV/at.), where $\tau_c = T/T_c$, $T_c = 1043$ K.

The ratios of the diffusion coefficients D_α/D_γ, D_γ/D_θ are 10^2–10^3 [51,52]; thus, the simulation with realistic diffusion coefficients is impossible, but the qualitative tendencies may be revealed when this ratio is chosen to be sufficiently large. We are also guided by the argument that relaxation of intermediate cementite to its stable state should have time to occur during the growth of the colony. Ultimately, we use the following coefficients: $D_\alpha/D_\gamma = D_\gamma/D_\theta = 10$.

The square size L is determined by its ratio to the interphase boundary width characterized by the parameter k_c, which is the same at the γ/α, γ/θ, and α/θ boundaries. We choose $k_c^2/(kTL^2) \approx 7 \times 10^{-4}$; in that case, according to estimations of the surface energy [53], the square side is $L \sim 1$ mkm.

[1] R. Abbaschian and R. Reed-Hill, *Physical Metallurgy Principles* (Cengage Learning, Stamford, 2009), p. 750.

[2] W. C. Leslie and E. Hornbogen, in *Physical Metallurgy*, edited by R. W. Cahn and P. Haasen (Elsevier, Amsterdam, 1996), Vol. 2, pp. 1555–1620.

[3] Fu-Wen Ling and D. E. Laughlin, The kinetics of transformation in Zn-Al superplastic alloys, *Metall. Trans. A* **10**, *921 (1979)*.

[4] A. T. Adorno, A. V. Benedetti, R. A. G. da Silva, and M. Blanco, Influence of the Al content on the phase transformation in Cu-Al-Ag alloys, Ecletica quimica **28**, 33 (2003).

[5] A. Das, W. Gust, and E. J. Mittemeijer, Eutectoid transformation in Au-39 at. % In, Mater. Sci. Technol. **16**, 593 (2000).

[6] C. Zener, Kinetics of decomposition of an austenite, Trans. AIME **167**, 550 (1946).

[7] M. Hillert, Solid state phase transformation, Jemkon. Ann. **141**, 757 (1957).

[8] D. Turnbull, Theory of cellular precipitation, Acta Metall. **3**, 55 (1955).

[9] J. W. Cahn, The kinetics of cellular segregation reactions, Acta Metall. **7**, 18 (1959).

[10] B. E. Sundquist, The edgewise growth of pearlite, Acta Metall. **16**, 1413 (1968).

[11] V. G. Vaks, A. Y. Stroev, V. N. Urtsev, and A. V. Shmakov, Experimental and theoretical study of the formation and growth of pearlite colonies in eutectoid steels, J. Exp. Theor. Phys. **112**, 961 (2011).

[12] A. Yamanaka, T. Yamamoto, T. Takaki, and Y. Tomita, in *Proceedings of IV International Conference Multiscale Materials Modeling (MMM)* (Florida State University, Tallahassee, FL, 2008), pp. 425–428.

[13] K. Ankit, A. Choudhury, C. Qin, S. Schulz, M. McDaniel, and B. Nestler, Theoretical and numerical study of lamellar eutectoid growth influenced by volume diffusion, Acta Mater. **61**, 4245 (2013).

[14] K. N. Tu and D. Turnbull, Morphology and structure of tin lamellae formed by cellular precipitation, Acta Metall. **17**, 1263 (1969).

[15] M. Hillert, in *Decomposition of Austenite by Diffusional Processes*, edited by V. F. Zackay and H. I. Aaronson (Interscience, New York, 1962), pp. 197–237.

[16] A. S. Pandit and H. K. D. H. Bhadeshia, Divorced pearlite in steels, Proc. R. Soc. A **468**, 2767 (2012).

[17] J. D. Verhoeven and E. D. Gibson, The divorced eutectoid transformation in steel, Metall. Mater. Trans. A **29**, 1181 (1998).

[18] T. Oyama, O. D. Sherby, J. Wadworth, and B. Walser, Application of the divorced eutectoid transformation to the development of fine-grained, spheroidized structures in ultrahigh carbon steels, Scr. Metall. **18**, 799 (1984).

[19] K. Ankit, R. Mukherjee, T. Mittnacht, and B. Nestler, Deviations from cooperative growth mode during eutectoid transformation: insights from phase field approach, Acta Mater. **81**, 204 (2014).

[20] K. Ankit, R. Mukherjee, and B. Nestler, Deviations from cooperative growth mode during eutectoid transformation: Mechanisms of polycrystalline eutectoid evolution in Fe-C steels, Acta Mater. **97**, 316 (2015).

[21] U. Hecht, L. Granasy, T. Pusztai, B Böttger, M Apel, V. Witusiewicz, L. Ratke, J. De Wilde, L. Froyen, D. Camel, B. Drevet, G. Faivre, S. G. Fries, B. Legendre, and S. Rex, Multiphase solidification in multicomponent alloys, Mater. Sci. Eng. **46**, 1 (2004).

[22] R. Folch and M. Plapp, Quantitative phase-field modeling of two-phase growth, Phys. Rev. E **72**, 011602 (2005).

[23] K. R. Elder, F. Drolet, J. M. Kosterlitz, and M. Grant, Stochastic Eutectic Growth, Phys. Rev. Lett. **72**, 677 (1994).

[24] F. Drolet, K. R. Elder, M. Grant, and J. M. Kosterlitz, Phase-field modeling of eutectic growth, Phys. Rev. E **61**, 6705 (2000).

[25] H. Ramanarayan and T. Abinandanan, Grain boundary effects on spinodal decomposition. II. Discontinuous microstructures, Acta Mater. **52**, 921 (2004)

[26] H. K. D. H. Bhadeshia, Carbon-carbon interactions in iron, J. Mater. Sci. **39**, 3949 (2004).

[27] I. K. Razumov, Yu. N. Gornostyrev, and M. I. Katsnelson, Effect of magnetism on kinetics of γ-α transformation and pattern formation in iron, J. Phys. Condens. Matter **25**, 135401 (2013).

[28] I. K. Razumov, D. V. Boukhvalov, M. V. Petrik, V. N. Urtsev, A. V. Shmakov, M. I. Katsnelson, and Yu. N. Gornostyrev, Role of magnetic degrees of freedom in a scenario of phase transformations in steel, Phys. Rev. B **90**, 094101 (2014).

[29] X. Zhang, T. Hickel, J. Rogal, S. Fähler, R. Drautz, and J. Neugebauer, Structural transformations among austenite, ferrite and cementite in Fe-C alloys: A unified theory based on *ab initio* simulations, Acta Mater. **99**, 281 (2015).

[30] P. M. Marcus, V. L. Moruzzi, and S. L. Qiu, Tetragonal equilibrium states of iron, Phys. Rev. B **60**, 369 (1999).

[31] S. V. Okatov, A. R. Kuznetsov, Yu. N. Gornostyrev, V. N. Urtsev, and M. I. Katsnelson, Effect of magnetic state on the γ-α transition in iron: First-principles calculations of the Bain transformation path, Phys. Rev. B **79**, 094111 (2009).

[32] C. S. Smith, Microstructure, Trans. Am. Soc. Met. **45**, 533 (1953).

[33] A. G. Khachaturyan, *Theory of Structural Transformations in Solids* (Dover, New York, 2008), p. 592.

[34] J. S. Smart, *Effective Field Theories of Magnetism* (Saunders, Philadelphia, 1968), p. 188.

[35] S. V. Okatov, Yu. N. Gornostyrev, A. I. Lichtenstein, and M. I. Katsnelson, Magnetoelastic coupling in γ-iron, Phys. Rev. B **84**, 214422 (2011).

[36] K. F. Laneri, J. Desimoni, and G. J. Zarragoicoechea, and A. Fernandez-Guillermet, Distribution of interstitials in fcc iron-carbon austenite: Monte Carlo simulations versus Mossbauer analysis, Phys. Rev. B **66**, 134201 (2002).

[37] B. M. Mogutnov, I. A. Tomilin, and L. A. Shvartsman, *Thermodynamics of Carbon-Iron Alloys* (Metallurgy, Moscow, 1972), p. 328 (in Russian).

[38] L. Battezzati, M. Baricco, and S. Curiotto, Non-stoichiometric cementite by rapid solidification of cast iron, Acta Mater. **53**, 1849 (2005).

[39] J. S. Darken and R. W. Gurry, Free Energy of Formation of Cementite and the Solubility of Cementite in Austenite, J. Met. **3**, 1015 (1951).

[40] A. Dick, F. Körmann, T. Hickel, and J. Neugebauer, *Ab initio* based determination of thermodynamic properties of cementite including vibronic, magnetic, and electronic excitations, Phys. Rev. B **84**, 125101 (2011).

[41] C. M. Fang, M. H. F. Sluiter, M. A. van Huis, C. K. Ande, and H. W. Zandbergen, Origin of Predominance of Cementite among Iron Carbides in Steel at Elevated Temperature, Phys. Rev. Lett. **105**, 055503 (2010).

[42] K. G. F. Janssens, D. Raabe, E. Kozeschnik, M. A. Miodovnik, and B. Nestler, *Computational Materials Engineering: An Introduction to Microstructure Evolution* (Elsevier, Amsterdam, 2007), p. 360.

[43] A. Hultrgen, Isothermal transformation of austenite, Trans. Am. Soc. Met. **39**, 915 (1947).

[44] M. M. Aranda, R. Rementeria, C. Capdevila, and R. E. Hackenberg, Can pearlite form outside of the Hultgren extrapolation if the Ae_3 and Acm phase boundaries, Metall. Mater. Trans. A **47**, 649 (2016).

[45] I. K. Razumov, The simulation of the growth of colonies in the spinodal decomposition of metastable phases, Russ. J. Phys. Chem. **83**, 1682 (2009).

[46] R. E. Smallman and R. J. Bishop, *Metals and Materials: Science, Processes, Applications* (Elsevier, Amsterdam, 2013), p. 444.

[47] V. M. Schastlivtsev, D. A. Mirzaev, and I. L. Yakovleva, *Pearlite in Carbon Steels* (Nauka, Ekaterinburg, 2006), p. 311 (in Russian).

[48] D. E. Jiang and Emily A. Carter, Carbon dissolution and diffusion in ferrite and austenite from first principles, Phys. Rev. B **67**, 214103 (2003).

[49] H. I. Aaronson, H. A. Domian, and G. P. Pound, Thermodynamics of the austenite—Proeutectoide ferrite transformation, Trans. Metall. Soc AIME **236**, 753 (1966).

[50] A. V. Ponomareva, Yu. N. Gornostyrev, and Igor Abrikosov, Energy of interaction between carbon impurities in paramagnetic γ-iron, Phys. Rev. B **90**, 014439 (2014).

[51] A. D. LeClaire, *Diffusion of C, N, and O in metals*, Landolt-Börnstein New Series Vol. III/26 (Springer-Verlag, Berlin, 1990), p. 471.

[52] B. Ozturk, The diffusion coefficient of carbon in cementite, Fe_3C, at 450 °C, Solid State Ionics **12**, 145 (1984).

[53] S. Kartha, J. A. Krumhansl, J. P. Sethna, and L. K. Wickham, Disorder-driven pretransitional tweed pattern in martensitic transformations, Phys. Rev. B **52**, 803 (1995).